Progress In Electromagnetics Research, PIER 79, 291–304, 2008

RAMAN AMPLIFICATION AND SUPERLUMINAL PROPAGATION OF ULTRAFAST PULSES BASED ON LOOP SILICON WAVEGUIDES: THEORETICAL MODELING AND PERFORMANCE

J.-W. Wu, F.-G. Luo, and Q.-T. Zhang

Institute of Optoelectronics Science and Engineering
and Wuhan National Laboratory for Optoelectronics
Huazhong University of Science and Technology
Wuhan 430074, P. R. China

Abstract—In this paper, we report, for the first time to the best of our knowledge, the detailed modeling and performance of Raman amplification and superluminal propagation of weak ultrafast femtosecond optical pulses in nonlinear loop single mode silicon-on-insulator anomalously dispersive optical waveguides. Using the device, theoretical results for 100-fs signal optical pulse show that when the launch peak power of signal pulse is fixed at -10 dBm, the gain value up to 30 dB can be achieved, and the delay time of superluminal propagation can also be adjusted by changing the system parameters, including initial chirp and peak power of pump pulse, initial delay time between pump and signal pulses, and waveguide length, etc.

1. INTRODUCTION

A nonlinear optical loop mirror (NOLM) that is a basic element in optics communications which is often selected for wavelength conversion [1], optical switch [2], and mode-locked laser [3], and so on. Usually, it basically consists of an optical fiber loop connected with a coupler for input and output. In the original design, the coupler splits unequally the input power so that the two counter-propagating components in the loop acquire different phase shifts. The difference in the acquired nonlinear phase depends on the input power level and fiber length. In fact, in order to create a useful device, several kilometers of fiber are required as a result that the NOLM implemented based optical fiber waveguide is impossible for integrated optics. Therefore, in our article, we design and present a modeling of NOLM based on the

integrated silicon-on-insulator (SOI) optical waveguide with only the length of several millimeters or centimeters that is promising candidate for integrated optoelectronics. As a transmission medium, SOI has much higher nonlinear effects than the commonly used silicon dioxide, and can confine the optical field to an area that is approximately 100 times smaller than modal area in a standard single mode optical fiber owing to high index contrast ratio between the core and cladding. In particular, the gain coefficient for Stimulated Raman Scattering (SRS) is approximately 10^4 times higher in silicon than in silica so that it is possible to produce light emission and amplification from SRS in SOI waveguides [4–10]. Another attractive issue is that the superluminal optical pulse propagation can be achieved in anomalously dispersive silicon waveguides for ultrafast femtosecond pulses. Moreover, the delay of output signal pulse can be controlled by changing the pump parameters such as initial chirp, peak power, and initial delay time between pump and signal pulses. Notice that superluminal pulse propagation can not be obtained for pulsewidth of picosecond or nanosecond because the influence of group velocity dispersion is ignored in these cases. In this paper, a nonlinear loop silicon waveguide device is designed and demonstrated theoretically which has some prominent advantages, i.e., higher gain level, for output signal pulse, can be obtained due to constructive interference at the output port comparing to the case in the straight waveguide, and the output pump and signal pulses that can be separated automatically after going through a round distance as a result of symmetric coupler in the device. In addition, the superluminal propagation becomes realism for ultrafast femtosecond pulse in single mode anomalously dispersive SOI waveguides. In fact, superluminal has already been demonstrated in other anomalously dispersive media [11].

The paper is structured as follows: In Section 2, we present the theory equations for ultrafast pulse propagation in nonlinear loop silicon waveguides. In Section 3, we display the simulation results with variable parameters of pump pulse. Section 4 summarizes the work.

2. THEORETICAL MODELING

Light propagating in waveguides can be described by group velocity, v_g, which is written as:

$$v_g = \frac{c}{n + \omega dn/d\omega} \tag{1}$$

where c is the speed of light in vacuum, n is the material refractive index, ω is the angle frequency. Here, the superluminal pulse

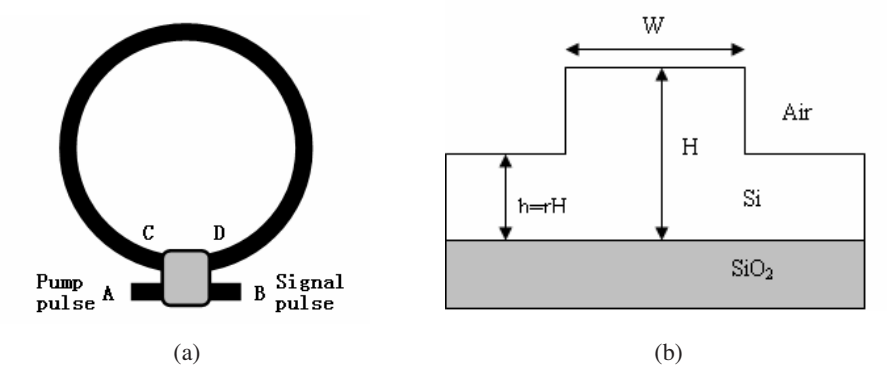

(a) (b)

Figure 1. Schematic diagrams of nonlinear loop silicon-on-insulator optical waveguide device and cross section.

propagation can be obtained when $dn/d\omega$ is negative.

As shown in Figure 1(a), the schematic diagram designed consists of a length of SOI waveguide in a loop via a symmetric coupler. By inspecting the schematic diagram, we can envision how optical pulses propagate in the whole device based on the device geometry. The pulses propagate along the SOI waveguide in both clockwise and counterclockwise directions. The input pump and signal pulses enter the device from the left leg A and right leg B, respectively, and then distributes evenly its power entering the loop device. Then, the counterpropagating waves travel along the loop and recombine at the coupler whose phase shifting of π is obtained because of even coupler. Finally, the pump pulse is completely outputted from the port A and the signal pulse is also reflected fully at port B such that they can be separated fully after going through the loop device. The cross section of a SOI rib waveguide that we adopted is shown in Figure 1(b) with width W, rib height H, and slab height h. These structures can be either single-mode or multimode depending on the ratio of the dimensions W/H and h/H. In our case we consider the single-mode condition, as follows [12]

$$\frac{W}{H} \leq \alpha + \frac{r}{\sqrt{1-r^2}} \tag{2}$$

and

$$0.5 \leq r \leq 1.0 \tag{3}$$

where r is the ratio of slab height to overall rib height, W/H is the ratio of waveguide width to overall rib height, and $\alpha = 0.3$.

In the remainder of this section, we will present the corresponding theoretical propagation equations. In this study, it is assumed that the temporal relationship between pump and signal pulses satisfies a Gaussian probability distribution as follows:

$$A_{p0} = \sqrt{P_{p0}} \exp\left[-\frac{1+iC_{p0}}{2}\left(\frac{T+T_{d0}}{T_{p0}}\right)^2\right] \tag{4}$$

$$A_{s0} = \sqrt{P_{s0}} \exp\left[-\frac{1+iC_{s0}}{2}\left(\frac{T}{T_{s0}}\right)^2\right] \tag{5}$$

where subscripts b and s denote the pump and signal pulses, respectively, A_0 is the slowly varying amplitude at the incident ports A or B, P_0 is the incident peak power, C_0 is the original chirp, $T$is the moving coordinate with the group velocity, T_0 is the half width at 1/e maximum intensity, T_{d0} is the delay time between pump and signal pulses before entering the loop device. The launch optical fields can be divided evenly into two parts by the symmetric coupler, and can be described by

$$\begin{bmatrix} A_p^+ \\ A_p^- \\ A_s^+ \\ A_s^- \end{bmatrix} = \begin{bmatrix} \sqrt{0.5} & 0 & 0 & 0 \\ 0 & i\sqrt{0.5} & 0 & 0 \\ 0 & 0 & i\sqrt{0.5} & 0 \\ 0 & 0 & 0 & \sqrt{0.5} \end{bmatrix} \begin{bmatrix} A_{p0} \\ A_{p0} \\ A_{s0} \\ A_{s0} \end{bmatrix} \tag{6}$$

where superscripts + and − denote the propagating optical fields along the clockwise and counterclockwise in loop device, respectively. According to literatures [13–17], the modified propagation equations of four optical waves in dispersive waveguides can be given by

$$\begin{aligned} &\frac{\partial A_p^+}{\partial z} + i\frac{1}{2}\beta_{p2}\frac{\partial^2 A_p^+}{\partial T^2} - \frac{1}{6}\beta_{p3}\frac{\partial^3 A_p^+}{\partial T^3} \\ &= -\frac{1}{2}\alpha_p A_p^+ - \frac{1}{2}\alpha_{FCA} A_p^+ \\ &\quad -\frac{1}{2}\beta_{TPA} g_{p,p}\left(\left|A_p^+\right|^2 + 2\left|A_p^-\right|^2\right)A_p^+ + i\gamma_{p,p}^+\left|A_p^+\right|^2 A_p^+ + i2\gamma_{p,s}^+\left|A_s^+\right|^2 A_p^+ \\ &\quad +i2\gamma_{p,p}^-\left|A_p^-\right|^2 A_p^+ + i2\gamma_{p,s}^-\left|A_s^-\right|^2 A_p^+ + i\frac{\omega_p}{c}\Delta n_p^+ A_p^+ \\ &\quad -\frac{1}{2}g_R^+\frac{\omega_p}{\omega_s}g_{p,s}^+\left|A_s^+\right|^2 A_p^+ - \frac{1}{2}g_R^-\frac{\omega_p}{\omega_s}g_{p,s}^-\left|A_s^-\right|^2 A_p^+ \end{aligned} \tag{7}$$

$$\begin{aligned}
&\frac{\partial A_p^-}{\partial z}+i\frac{1}{2}\beta_{p2}\frac{\partial^2 A_p^-}{\partial T^2}-\frac{1}{6}\beta_{p3}\frac{\partial^3 A_p^-}{\partial T^3}\\
=\;&-\frac{1}{2}\alpha_p A_p^- -\frac{1}{2}\alpha_{FCA}A_p^-\\
&-\frac{1}{2}\beta_{TPA}g_{p,p}\left(\left|A_p^-\right|^2+2\left|A_p^+\right|^2\right)A_p^- +i\gamma_{p,p}^-\left|A_p^-\right|^2 A_p^- +i2\gamma_{p,s}^-\left|A_s^-\right|^2 A_p^-\\
&+i2\gamma_{p,p}^+\left|A_p^+\right|^2 A_p^- +i2\gamma_{p,s}^+\left|A_s^+\right|^2 A_p^- +i\frac{\omega_p}{c}\Delta n_p^- A_p^-\\
&-\frac{1}{2}g_R^-\frac{\omega_p}{\omega_s}g_{p,s}^-\left|A_s^-\right|^2 A_p^- -\frac{1}{2}g_R^+\frac{\omega_p}{\omega_s}g_{p,s}^+\left|A_s^+\right|^2 A_p^- \qquad (8)
\end{aligned}$$

$$\begin{aligned}
&\frac{\partial A_s^+}{\partial z}+d\frac{\partial A_s^+}{\partial T}+i\frac{1}{2}\beta_{s2}\frac{\partial^2 A_s^+}{\partial T^2}-\frac{1}{6}\beta_{s3}\frac{\partial^3 A_s^+}{\partial T^3}\\
=\;&-\frac{1}{2}\alpha_s A_s^+ -\frac{1}{2}\alpha_{FCA}A_s^+\\
&-\frac{1}{2}\beta_{TPA}g_{p,p}\left(2\left|A_p^+\right|^2+2\left|A_p^-\right|^2\right)A_s^+ +i\gamma_{s,s}^+\left|A_s^+\right|^2 A_s^+ +i2\gamma_{s,p}^+\left|A_p^+\right|^2 A_s^+\\
&+i2\gamma_{s,s}^-\left|A_s^-\right|^2 A_s^+ +i2\gamma_{s,p}^-\left|A_p^-\right|^2 A_s^+ +i\frac{\omega_s}{c}\Delta n_s^+ A_s^+\\
&+\frac{1}{2}g_R^+ g_{s,p}^+\left|A_p^+\right|^2 A_s^+ +\frac{1}{2}g_R^- g_{s,p}^-\left|A_p^-\right|^2 A_s^+ \qquad (9)
\end{aligned}$$

$$\begin{aligned}
&\frac{\partial A_s^-}{\partial z}+d\frac{\partial A_s^-}{\partial T}+i\frac{1}{2}\beta_{s2}\frac{\partial^2 A_s^-}{\partial T^2}-\frac{1}{6}\beta_{s3}\frac{\partial^3 A_s^-}{\partial T^3}\\
=\;&-\frac{1}{2}\alpha_s A_s^- -\frac{1}{2}\alpha_{FCA}A_s^-\\
&-\frac{1}{2}\beta_{TPA}g_{p,p}\left(2\left|A_p^-\right|^2+2\left|A_p^+\right|^2\right)A_s^- +i\gamma_{s,s}^-\left|A_s^-\right|^2 A_s^- +i2\gamma_{s,p}^-\left|A_p^-\right|^2 A_s^-\\
&+i2\gamma_{s,s}^+\left|A_s^+\right|^2 A_s^- +i2\gamma_{s,p}^+\left|A_p^+\right|^2 A_s^- +i\frac{\omega_s}{c}\Delta n_s^- A_s^-\\
&+\frac{1}{2}g_R^- g_{s,p}^-\left|A_p^-\right|^2 A_s^- +\frac{1}{2}g_R^+ g_{s,p}^+\left|A_p^+\right|^2 A_s^- \qquad (10)
\end{aligned}$$

where the coefficients in the equations (7)–(10) are defined as

$$\gamma_{i,i} = \frac{\omega_i}{2cn_{eff}}g_{i,i}\left(\chi_{xxxx}^{NR}+\chi^R(0)\right) \qquad (11)$$

$$\gamma_{i,j} = \frac{\omega_i}{2cn_{eff}}g_{i,j}\left(\chi_{xxyy}^{NR}\right) \qquad (i\neq j) \qquad (12)$$

where n_{eff} is the effective index, χ_{xxxx}^{NR} ($=0.5\times10^{-18}\,\mathrm{m^2V^{-2}}=2\chi_{xxyy}^{NR}$ [18]) is the electronic non-resonant susceptibility. χ^R the Raman

resonant susceptibility can be written as

$$\chi^R(\omega_{s0};\omega_p-\omega_{s0},\omega_{s0})=\frac{2\Omega_R\Gamma_R\xi_R}{2i\Gamma_R\Delta\omega+\Omega_R^2-\Delta\omega^2} \tag{13}$$

where Ω_R (= 15.6 THz) is the Raman frequency shift, ξ_R (= $11.2\times10^{-18}\,\mathrm{m^2V^{-2}}$) is the Raman susceptibility when $\Delta\omega=\Omega_R$, Γ_R (= $2\pi\times53\,\mathrm{GHz}$) is the resonance half-width [18]. The overlap integrals $g_{i,j}$ is given by

$$g_{i,j}=\frac{\iint|F_i(x,y)|^2\,|F_j(x,y)|^2dxdy}{\iint|F_i(x,y)|^2\,dxdy\iint|F_j(x,y)|^2\,dxdy} \tag{14}$$

In Equations (7)–(10) d is the mismatch of group velocity between pump and signal pulses, β_2 and β_3 are the group velocity and third-order dispersion, α is the propagation loss parameter, β_{TPA} is the two-photon absorption parameter, α_{FCA}, and Δn indicate respectively the free-carrier absorption parameter, the change of effective index due to the free-carrier dispersion, and can be written as [19, 20]

$$\begin{aligned}\alpha_{FCA}&=8.5\times10^{-18}\cdot\left(\frac{\lambda_{p,s}}{1.55}\right)^2\Delta n_e+6.0\times10^{-18}\cdot\left(\frac{\lambda_{p,s}}{1.55}\right)^2\Delta n_h\\&=\sigma\cdot n\\&=\sigma_0\cdot\left(\frac{\lambda_{p,s}}{1.55}\right)^2 n\end{aligned} \tag{15}$$

$$\Delta n=-8.8\times10^{-22}\cdot\left(\frac{\lambda_{p,s}}{1.55}\right)^2\Delta n_e-8.5\times10^{-18}\cdot\left(\frac{\lambda_{p,s}}{1.55}\right)^2(\Delta n_h)^{0.8} \tag{16}$$

where $n=n_e=n_h$ is the density of electron-hole pairs generated by the two-photon absorption process. The coefficient $\sigma_0=1.45\times10^{-17}\,\mathrm{cm^2}$ [21] is the free-carrier absorption cross section measured at $\lambda=1.55\,\mu$m.

To obtain a consistent mathematical model, the Equation (5) has been coupled to the rate equation governing the free carrier dynamic into the waveguide, given by [7]

$$\frac{dn}{dT}=-\frac{n}{\tau_{eff}}+\frac{\beta_{TPA}}{2\hbar\omega_p}g_{p,p}^2\left[(A_p^+ + A_p^-)^2\right]^2 \tag{17}$$

where n is the carriers density, $\hbar$ is the reduced Planck constant, and τ_{eff} is the relevant effective recombination lifetime for free carrier,

denoted by [22]

$$\tau_{eff}^{-1} = \frac{S}{H} + \frac{w + 2(H-h)}{wH} S' + 2\frac{h}{H}\sqrt{\frac{D}{w^2}\left(\frac{S+S'}{h}\right)} \tag{18}$$

where the first term refers to the interface recombination lifetime, the second term refers to the surface recombination at the sidewalls, and last term refers to transit time out of the modal area. S and S' are the effective surface recombination velocity, D is diffusion coefficient.

To simulate the propagation of signal pulse in loop device and the output properties of amplified signal pulse at port B, the propagation equations (7)–(10) can be solved numerically by the well-known finite-difference time-domain (FDTD) method [23–26]. Finally, at port B, the amplitude of the output amplified signal pulse can be given by

$$A_{sout} = \sqrt{0.5}A_{sL}^{+} + i\sqrt{0.5}A_{sL}^{-} \tag{19}$$

where A_{sout} is the output amplitude, A_{sL}^{+}, and A_{sL}^{-} are the amplitudes of A_s^{+}, and A_s^{-}, respectively, after going through a round distance of loop device.

3. RESULTS AND DISCUSSIONS

In this section we study the Raman amplification and superluminal propagation of weak ultrafast femtosecond pulses. According to literatures [22, 27–29], the system parameters may be determined in calculations: $D = 16\,\mathrm{cm}^2 \cdot \mathrm{s}^{-1}$, $c = 2.99792458 \times 10^8\,\mathrm{m} \cdot \mathrm{s}^{-1}$, $n_{eff} = 2.83$, $\hbar = 1.0552 \times 10^{-34}\mathrm{J} \cdot \mathrm{s}^{-1}$, $\lambda_p = 1.55\,\mu\mathrm{m}$, $\lambda_s = 1.67\,\mu\mathrm{m}$, $\alpha = 0.22\,\mathrm{dB{\cdot}cm}^{-1}$, $\beta_{TPA} = 0.5\,\mathrm{cm{\cdot}GW}^{-1}$, $g_R = 10.5 \times 10^{-9}\,\mathrm{cm{\cdot}GW}^{-1}$, $S, S' = 80\,\mathrm{m} \cdot \mathrm{s}^{-1}$, $\beta_{2p} = -2\,\mathrm{ps}^2\mathrm{m}^{-1}$, $\beta_{2s} = -1\,\mathrm{ps}^2\mathrm{m}^{-1}$, $\beta_{3p} = 0.002\,\mathrm{ps}^3\mathrm{m}^{-1}$, $\beta_{3s} = -0.002\,\mathrm{ps}^3\mathrm{m}^{-1}$, $W = 450\,\mathrm{nm}$, $H = 500\,\mathrm{nm}$, $h = 320\,\mathrm{nm}$, $T_0 = 100\,\mathrm{fs}$.

Figure 2 shows the normalized shapes of output signal and reference pulses at port B after transmitting a loop distance. The peak powers of input signal and pump pulses corresponds to $-10\,\mathrm{d}\beta\mathrm{m}$, and $34.77\,\mathrm{d}\beta\mathrm{m}$, respectively. The initial delay time is 200-fs, namely, the incident signal pulse lags the incident pump pulse. $C_p = 2$ is chosen. We choose $C_s = 0$ as a invariable value for all of our calculations. As seen in Figure 2, the output superluminal propagation pulse becomes asymmetric such that its leading edge is shaper compared with the trailing edge. Sharpening of the leading edge occurs because the leading edge experiences larger velocity than the trailing edge. The reference pulse is plotted without considering the effects of group

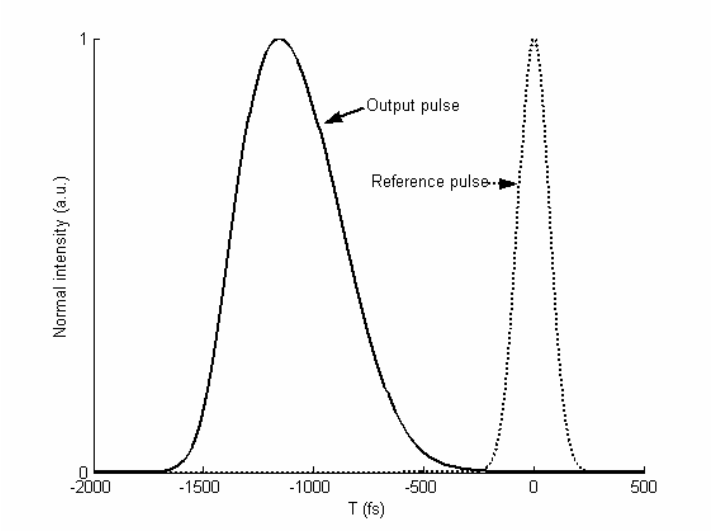

Figure 2. The normalized shapes of output signal and reference pulses after 15-mm loop.

velocity dispersion and free carrier dispersion. When considering effects of all linear and nonlinear, the output signal pulse is before the reference pulse, i.e., the output pulse's velocity is larger than that of reference pulse. The phenomenon can be explained that the change of effective index is always negative according to Equation (16), and the variation of angle frequency $d\omega$ is positive over the total pulse which is displayed in Figure 3. As a result, the behavior of superluminal propagation is realized according to the expression of group velocity in Equation (1). Note that the pulsewidth broadens due to the influence of group velocity dispersion. In the following parts, we will discuss in detail the properties of amplified output pulse, including the Raman gain, pulsewidth, and delay time, with variable initial chirp, initial delay, and loop length.

Figures 4(a), (b), and (c) show the time domain properties and superluminal propagations of output signal pulses versus the initial chirp of pump pulse from the loop device with variable loop length and initial delay time. From Figures 4(a) to (c), the same type curves stand for the identical pulse. In Figure 4(a), we can see that the Raman gain value up to $30\,\mathrm{d}\beta$ is obtained owing to the constrictive interference that occurs as a result of the symmetric coupler in the loop device which is larger than the same long straight waveguide. Note also that when the initial chirp C_p is positive. With the increase

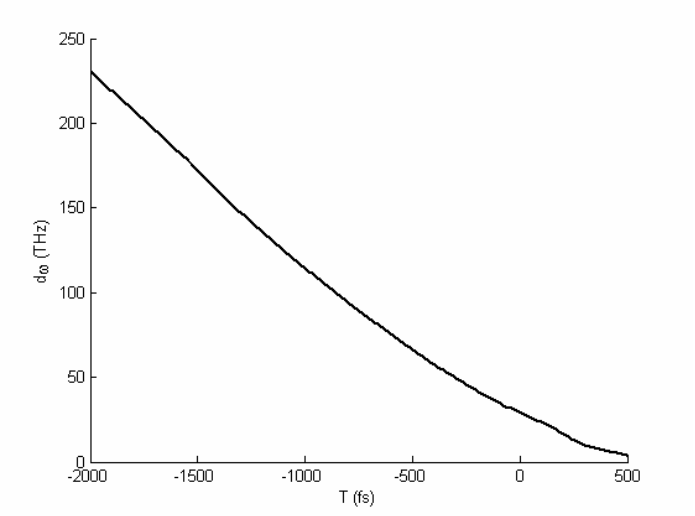

Figure 3. The change of angle frequency of output signal pulse across the total pulse.

of C_p, the Raman gain will experience the almost linearly increase from SRS then decay slowly rooting in the gain saturation and linear and nonlinear losses with initial delay time $T_d > 0$. Some noteworthy features of the Raman gain curves are that when the value of $C_p > 1$, the gain is insensitive to the C_p because of gain saturation, i.e., pump depletion, and when the case of $C_p < 0$, the gain level is low comparing to the $C_p > 1$ for the same pulse because the pump pulse will broaden linearly in waveguide of anomalous dispersion with $\beta_{2p}C_p > 0$, on the contrary, when the case $\beta_{2p}C_p < 0$, the pump pulse will narrow then broaden as a result that the gain level is increased. In general, the Raman gain of output signal pulse is strongly dependent on the initial delay time and loop length. Simultaneously, the pulsewidths are sub-linearly increasing for $C_p > 0$, however, whose variation are complex for $C_p < 0$ which are displayed in Figure 4(b). These phenomena are mainly controlled by the influence of group velocity dispersion. In addition, the superluminal propagation is a very important physical phenomenon in anomalous dispersion waveguide and is demonstrated in our designed device whose the delay curves are plotted in Figure 4(c). As seen in the figure, the absolute delay time sub-linearly increases with the increase of C_p because the sign of the changes of angle frequency, $d\omega$, always hold on positive and lead to increased group velocity. If we increase the initial delay time T_{d0}, the absolute delay time of output pulse will also be increased. But, to hold large Raman gain, both of

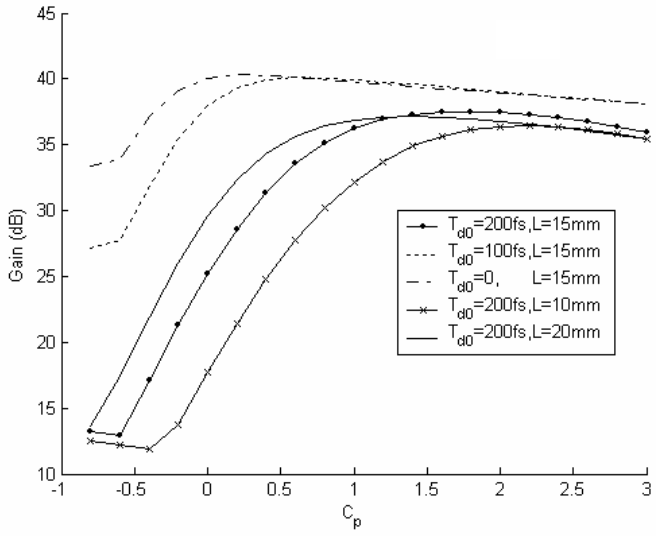
Gain (dB)
C_p
T_{d0}=200fs,L=15mm
T_{d0}=100fs,L=15mm
T_{d0}=0, L=15mm
T_{d0}=200fs,L=10mm
T_{d0}=200fs,L=20mm

(a)

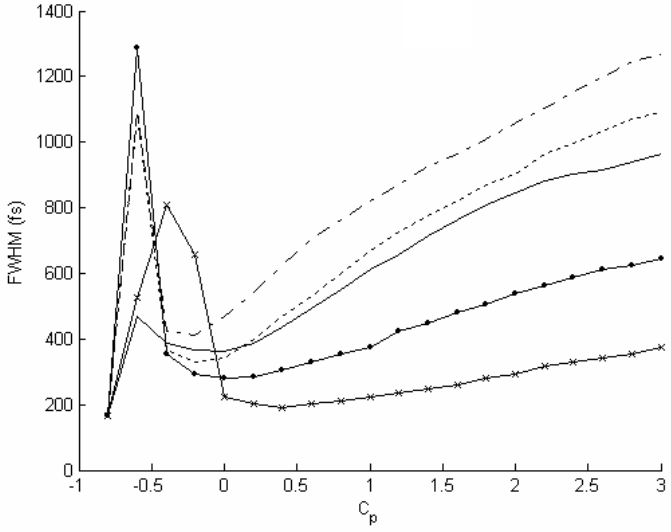
FWHM (fs)
C_p

(b)

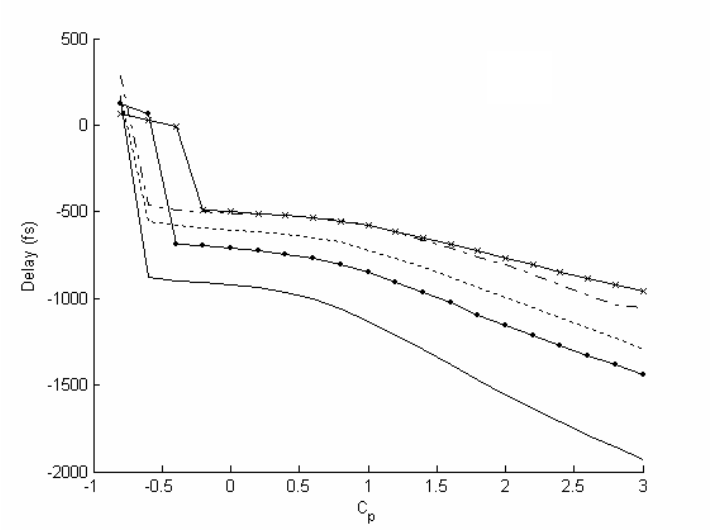

(c)

Figure 4. The Raman gains (a), full width at half maximum (FWHM) (b), and delay times (c) of output signal pulse as a function of initial chirp of pump pulse with different initial delay time and loop length.

the input pulses must overlap during the propagation so that the initial delay time should locate in a suitable range.

4. CONCLUSIONS

This paper has presented a theoretical modeling and performance of nonlinear loop device based on silicon-on-insulator optical waveguide and symmetric coupler. Numerical results find that the Raman gain value up to $30\,\mathrm{d}\beta$ and superluminal ultrafast pulse propagation can be achieved in our designed modeling if the anomalous dispersion is satisfied for silicon waveguide. In particular, the properties of output signal strongly depend on the initial chirp of pump pulse, initial delay time between launch two pulses, and loop length, etc. which should be specifically adjusted to obtain larger Raman gain and absolute delay time within a fixed loop length.

ACKNOWLEDGMENT

This work was supported by the Chinese Natural Science Foundation under grant No. 60677023.

REFERENCES

1. Yu, J., Y. Qian, P. Jeppesen, and S. N. Knudsen, "Broad-band and pulsewidth-maintained wavelength conversion based on a high-nonlinearity DSF nonlinear optical loop mirror," *IEEE Photon. Technol.*, Vol. 13, No. 4, 344–346, 2001.
2. Shi, H., "Performance analysis on semiconductor laser amplifier loop mirrors," *J. of Lightwave Technol.*, Vol. 20, No. 4, 682–688, 2002.
3. Sun, H., H. Dong, and N. K. Dutta, "Mode-locked erbium-doped fiber ring laser using intracvity polarization-maintaining loop mirror," *IEEE Photon. Technol.*, Vol. 18, No. 12, 1311–1313, 2006.
4. Rong, H., A. Liu, R. Jones, O. Cohen, D. Hak, R. Nicolaescu, A. Fang, and M. Paniccia, "An all-silicon Raman laser," *Nature*, Vol. 433, No. 17, 292–294, 2005.
5. Rong, H., R. Jones, A. Liu, O. Cohen, D. Hak, A. Fang, and M. Paniccia, "A continuous-wave Raman silicon laser," *Nature*, Vol. 433, No. 20, 725–728, 2005.
6. Liang, T. and H. Tsang, "Efficient Raman amplification in silicon-on-insulator waveguide," *Appl. Phys. Lett.*, Vol. 85, No. 16, 3343–3345, 2004.
7. Liu, A., H. Rong, R. Jones, O. Cohen, D. Hak, and M. Paniccia, "Optical amplification and lasing by stimulated Raman scattering in silicon waveguides," *J. of Lightwave Technol.*, Vol. 24, No. 3, 1440–1455, 2006.
8. Xu, Q., V. R. Almelda, and M. Lipson, "Demonstration of high Raman gain in a submicrometer-size silicon-on-insulator waveguide," *Opt. Lett.*, Vol. 30, No. 1, 35–37, 2005.
9. Liu, A., H. Rong, and M. Paniccia, "Net optical gain in a low loss silicon-on-insulator waveguide by stimulated Raman scattering," *Opt. Express*, Vol. 12, No. 8, 4261–4268, 2004.
10. Wu, J. W. and F. G. Luo, "Generation of high repetition rate picosecond pulse train based on ultra-small silicon waveguide," *Progress In Electromagnetics Research*, PIER 75, 163–170, 2007.
11. Dogariu, A., A. Kuzmich, H. Cao, and L. J. Wang, "Superluminal light pulse propagation via rephrasing in a transparent anomalously dispersive medium," *Opt. Express*, Vol. 8, No. 6, 344–350, 2001.
12. Lousteau, J., D. furniss, A. B. Scddon, T. M. Benson, A. Vukovic, and P. Sewell, "The single-mode condition for silicon-on-insulator optical rib waveguides with large cross section," *J. of Lightwave*

Technol., Vol. 22, No. 8, 1923–1929, 2006.

13. Leonardis, F. D. and V. M. N. Passaro, "Modeling of Raman amplification in silicon-on-insulator optical microcavities," *New J. of Phys.*, Vol. 9, No. 25, 1–24, 2007.
14. Leonardis, F. D. and V. M. N. Passaro, "Modeling and performance of a guided-wave optical angular-velocity sensor based on Raman effect in SOI," *J. of Lightwave Technol.*, Vol. 25, No. 9, 2352–2366, 2007.
15. Shwetanshumala, S. A. Biswas, and S. Konar, "Dynamically stable super Gaussian solitons in semiconductor doped glass fibers," *J. of Electromagn. Waves and Appl.*, Vol. 20, No. 7, 901–912, 2006.
16. Biswas, A., S. Konar, and E. Zerrad, "Soliton-soliton interaction with parabolic law nonlinearity," *J. of Electromagn. Waves and Appl.*, Vol. 20, No. 7, 927–939, 2006.
17. Biswas, A., Shwetanshumala, and S. Konar, "Dynamically stable dispersion-managed optical solitons with parabolic law nonlinearity," *J. of Electromagn. Waves and Appl.*, Vol. 20, No. 9, 1249–1258, 2006.
18. Dimitropoulos, D., V. Raghunathan, R. Claps, and B. Jalali, "Phase-matching and nonlinear optical processes in silicon waveguides," *Opt. Express*, Vol. 12, No. 1, 149–160, 2003.
19. Passaro, V. M. N. and F. D. Leonardis, "Space-time modeling of Raman pulses in silicon-on-insulator optical waveguides," *J. of Lightwave Technol.*, Vol. 24, No. 7, 2920–2931, 2006.
20. Soref, R. A. and B. R. Bennett, "Electrooptical effects in silicon," *IEEE Quantum Electron.*, Vol. QE-23, No. 1, 123–129, 1987.
21. Claps, R., V. Rahgunathan, D. Dimitropoulos, and B. Jalali, "Influence of nonlinear absorption on Raman amplification in silicon waveguides," *Opt. Express*, Vol. 12, No. 12, 2774–2780, 2004.
22. Dimitropoulos, D., R. Jhaveri, R. Claps, J. C. S. Woo, and B. Jalali, "Lifetime of photogenerated carriers in silicon-on-insulator rib waveguides," *Appl. Phys. Lett.*, Vol. 86, No. 3, 071115(1–3), 2005.
23. Chen, X., D. Liang, and K. Huang, "Micro wave imaging 3-D buried objects using parallel gentic algorithm combined with FDTD technique," *J. of Electromagn. Waves and Appl.*, Vol. 20, No. 13, 1761–1774, 2006.

24. Gong, Z. Q. and G. Q. Zhu, "FDTD analysis of an anisotropically coated missile," *Progress In Electromagnetics Research*, PIER 64, 69–80, 2006.
25. Khalaj-Amirhosseini, M., "Analysis of lossy inhomogeneous planar layers using finite difference method," *Progress In Electromagnetics Research*, PIER 59, 187–198, 2006.
26. Luo, S. and Z. D. Chen, "An efficient modal FDTD for absorbing boundary conditions and incident wave generator in waveguide structures," *Progress In Electromagnetics Research*, PIER 68, 229–246, 2007.
27. Raghunathan, V., R. Claps, D. Dimitropoulos, and B. Jalali, "Parametric Raman wavelength conversion in scaled silicon waveguides," *J. of Lightwave Technol.*, Vol. 23, No. 6, 2094–2101, 2005.
28. Hsieh, I. W., X. Chen, J. I. Dadap, N. C. Panoin, R. M. Osgood, S. J. Mcnab, and Y. A. Vlasov, "Itrafast-pulse self-phase modulation and third-order dispersion in Si photonic wire-waveguides," *Opt. Express*, Vol. 14, No. 25, 12380–12387, 2006.
29. Yin, L. and G. P. Agrawal, "Impact of two-photon absorption on self-phase modulation in silicon waveguides," *Opt. Lett.*, Vol. 32, No. 4, 2031–2033, 2007.